Influence of Al content in the barrier on the optical properties of GaAs/$Al_xGa_{1-x}As$ ($x=0.1-1$) multiple-quantum-well structures

Nguyen Hong Ky, J. D. Ganière, M. Gailhanou, F. Morier-Genoud, D. Martin, and F. K. Reinhart
Institute for Micro- and Optoelectronics, Swiss Federal Institute of Technology, CH-1015 Lausanne, Switzerland
(Received 18 February 1992)

GaAs/$Al_xGa_{1-x}As$ multiple-quantum-well structures with identical well thicknesses (≈ 110 Å) but with different Al contents x in the barrier ($x \approx 0.1$, 0.2, 0.45, and 1) were grown by molecular-beam epitaxy. We report the characterization of the structures by a combination of different techniques. The x-ray-diffraction technique allows us to estimate the Al content x and to measure the period of the structure with good accuracy. Using the photographs given by high-resolution transmission electron microscopy on cleaved wedges, we investigate directly the key parameters of the structures, such as the regularity, the layer thickness, and the Al content x. The photoluminescence measurements carried out in detail from 4 K to room temperature show the excitonic character of the radiative recombination in these structures up to room temperature. The influence of x on the photoluminescence is investigated systematically. The data confirm the theoretical results calculated using finite barrier heights. The increase of transition energies with increasing x is due to the increase of confinement energies and exciton binding energies. A good agreement of the structure parameter values obtained by the above techniques is given.

I. INTRODUCTION

Characterization of semiconductor quantum-well (QW) structures is very important for the development of optoelectronic devices based on the quantum size effect.[1] The advancement of QW structures is correlated to the progress in the characterization. X-ray diffraction is a practical and nondestructive method which is very convenient to measure the average Al content x_{av}, the quantum-well layer thickness L_w, and the barrier layer thickness L_b of the QW structures.[1-3] Using x-ray diffraction, we can also evaluate the quality of the material and the uniformity of the structure. Transmission electron microscopy on a cleaved wedge of the sample (WTEM) is a technique in specimen preparation and observation proposed by Kakibayashi and Nagata.[4] This local technique is very interesting due to its simplicity in specimen preparation and its potential for high-resolution observation. It has been intensively developed for studying morphology and chemical composition of the epitaxial $Al_xGa_{1-x}As$/GaAs layers grown by molecular-beam epitaxy (MBE) or metal-organic vapor phase epitaxy (MOVPE).[5-8] Using this method, we obtain rapidly the information about the layer thickness, the Al content x, the spatial extension of the interfaces, and the composition fluctuation in the epitaxial layers. Photoluminescence (PL) measurements have been widely used in recent years to investigate the multiple-quantum-well (MQW) structures. A number of papers have reported on the excitonic properties and temperature behavior of the PL of GaAs/$Al_xGa_{1-x}As$ multiple-quantum-well structures. For high-quality QW's, because of the increase of the exciton binding energy due to the spatial confinement, the exciton recombination can be observed even at room temperature.[9-12] Electrons and holes in GaAs layers are confined in potential wells whose heights depend on the Al content x of the surrounding $Al_{1-x}Ga_xAs$ layers. The influence of the barrier height on properties of MQW structures has been studied theoretically. Bastard[13] reported that the dominant effect in quantum-well energy levels is the finiteness of the barrier height. Greene, Bajaj, and Phelps[14] found that both the magnitude and the qualitative behavior of the exciton binding energies calculated using finite barrier heights are very different from those obtained using an infinite potential barrier.

In this paper, we report a combined characterization of the MBE-grown GaAs/$Al_xGa_{1-x}As$ MQW structures with the same L_w and L_b, but the Al content in the barrier varies ($x \approx 0.1$, 0.2, 0.45, and 1). We investigate experimentally the influence of the Al content x in the barrier on the PL properties of the MQW structures. The sample description and the experimental setup are reported in Sec. II. We give the characterization results and discussions of the x-ray diffraction, the WTEM, and the PL measurements in Secs. III, IV, and V, respectively. The conclusion is given in Sec. VI.

II. EXPERIMENT

Four GaAs/$Al_xGa_{1-x}As$ MQW structures were grown by MBE on (001)-oriented GaAs:Si substrates. The growth temperature was 620 °C. At this growth temperature the diffusion of Si from the substrate into the epitaxial layers is negligible. The carrier concentration of unintentionally doped GaAs grown in our system is below 10^{15} cm^{-3}. All structures consist of the following undoped layers: a GaAs buffer layer, a MQW region with 30 GaAs wells separated by $Al_xGa_{1-x}As$ barriers, and a GaAs cap layer. The only difference between the structures is the Al content x of $Al_xGa_{1-x}As$ barriers which is expected to be $x=0.1$, 0.2, 0.45, and 1. In this paper, we will call our samples *A*, *B*, *C*, and *D* following the increasing order of x.

The x-ray-diffraction measurements were carried out

on a Philips HR1 high-resolution diffractometer. The two-crystals–four-reflections Ge monochromator was configured on its 220 setting that provides an intense parallel monochromatic beam (Cu $K\alpha 1, \lambda = 0.15406$ nm). The spot size was about $(5-10)\times 1.5$ mm^2 on the samples. (006) reflection rocking curves were used to determine the average Al content x_{av} of the MQW structures whereas the characterization of their periodicity was achieved using (002) reflection.

For WTEM characterization, we cleave along the (± 110) planes of the samples to produce a specimen with a perfect 90° wedge. The specimen is mounted on a homemade copper grid. The observation is done along the (100) zone axis, using a Philips EM-300 transmission electron microscope. The region transparent to electrons covers a distance of a few hundred nanometers from the edge.[6]

We use a standard PL experimental setup with the 6328-Å line of a helium-neon laser and the 5145-Å line of an argon-ion laser as excitation sources, and a Si photodiode as a detector. The exciting intensity of the laser beam is varied by neutral density filters in the range of 0.1–10 W/cm^2. The temperature of the samples was controlled by a PT100/1515 resistance with a resolution of ±0.5 K.

III. X-RAY DIFFRACTION CHARACTERIZATION

Figure 1 shows a (002) and a (006) reflection x-ray-diffraction rocking curve of sample *B*. The (002) rocking curve [Fig. 1(a)] displays a series of very sharp peaks.

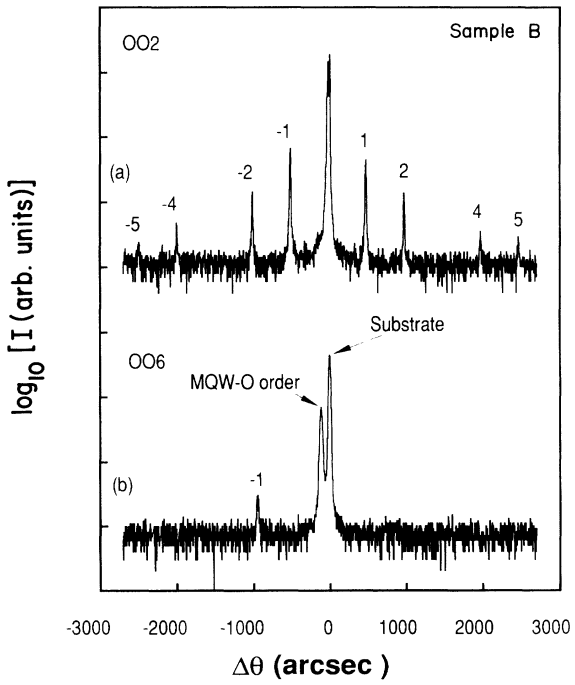

FIG. 1. X-ray-diffraction rocking curves of sample *B* using (a) (200) and (b) (600) reflection. The numbers indicate the diffraction orders.

The most intense peak corresponds to the GaAs substrate. The labeled satellite peaks are due to the different orders of diffraction of the MQW structure. Their narrowness gives evidence for the high uniformity of chemical composition and layer periodicity of the MQW structure over the 30 periods as well as laterally over the x-ray spot size.

The period of the MQW structure can be calculated from the angular separation of two diffraction satellite peaks,

$$L_b + L_w = \frac{\lambda(m-n)}{2[\sin(\theta_m)-\sin(\theta_n)]}\ , \tag{1}$$

where m and n are the diffraction orders of the two satellites, θ_m and θ_n—their respective angular positions, and λ the x-ray wavelength.

The angular separation $\Delta\theta_{o.s.}$ between the so-called zero-order satellite and the substrate peak allows the determination of the average Al content x_{av} of the MQW structures. To estimate this parameter, the (006) reflection is preferred over the (002) one due to its better resolution [Fig. 1(b)]. Recently published values of the Poisson coefficient ν and lattice parameter of AlAs (Refs. 15 and 16) were used for the calculation of x_{av}. The dependence of ν on Al composition was taken into account for $Al_xGa_{1-x}As$.

By assuming a constant Ga flux over the complete MQW growth, the Al content x of the $Al_xGa_{1-x}As$ barrier, the thickness of the wells, L_w, and the width of the barriers, L_b, can be calculated.

From the measured values $\Delta\theta_{o.s.}$ and θ_m, θ_n we determined x_{av}, x, L_b+L_w, and L_w for all samples *A*, *B*, *C*, and *D*. These values are given in Table I along with those obtained by WTEM and with those that give the best fit of PL data.

IV. WTEM CHARACTERIZATION

Figure 2 presents a WTEM photograph of sample *C* taken in a bright field. On the photograph, the black and white equal thickness fringes are observed near the edge of the samples. The position and the shape of the fringes depend on the chemical composition of the material. Discontinuities in the structure of the fringes reveal the layer interfaces.[5–8] The photographs confirm that the structure of all samples is identical: From the left side to the right side of each photograph we discern the GaAs cap layer, the MQW region consisting of 30 alternating GaAs wells and $Al_xGa_{1-x}As$ barriers, the GaAs buffer layer, and the AlAs marker that indicates the border between the substrate and the epitaxial layers. The sudden shift of fringes indicates that the interfaces of the layers are abrupt. This allows us to measure the layer thickness with a precision of some Å. Using the measured values of the layer thickness and the growth time, we determine x_{av} and x. The parameters of all MQW structures obtained by WTEM are given in Table I. The width of the fringes is largest in the AlAs layers, and it is smallest in the GaAs layers. The bending of the thickness fringes in the $Al_xGa_{1-x}As$ layers is due to an oxidation of $Al_xGa_{1-x}As$ under contact with air prior to the observa-

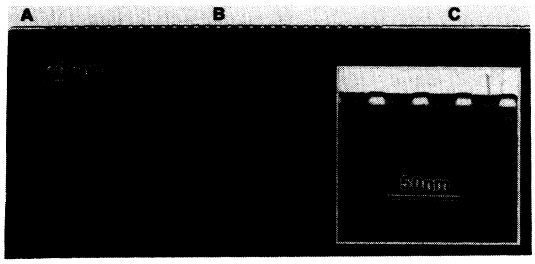

FIG. 2. WTEM photograph of sample *C*. The growth direction is from the right to the left. In this figure, the letter A indicates the GaAs cap layer, B the MQW region, and C the GaAs buffer layer.

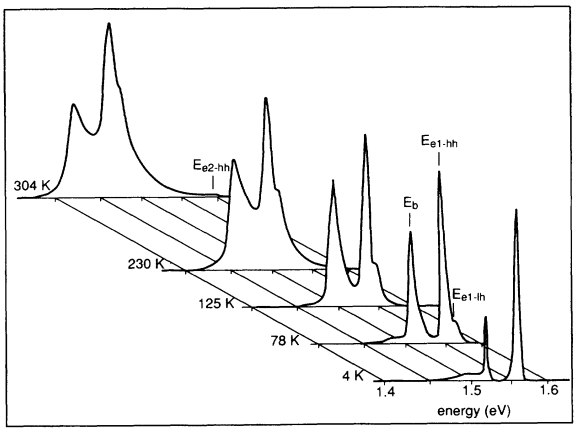

FIG. 3. Typical PL spectra of the sample *D* ($x=1$) taken at different temperatures. The labels on the spectra indicate the recombination of free excitons in the GaAs buffer layer (E_b), and the recombination of the $n=1$ electron–heavy-hole exciton ($E_{e1\text{-hh}}$), the $n=1$ electron–light-hole exciton ($E_{e1\text{-lh}}$), and the $n=2$ electron–heavy-hole exciton ($E_{e2\text{-hh}}$) in the wells. The lattice temperatures are marked on the left side of each plot.

tion. The oxide layer on the sample surface is very thin. From sample *D* to sample *A* the width and the bending of the fringes in the $Al_xGa_{1-x}As$ barriers decrease because the Al composition decreases from $x=1$ to $x\approx 0.1$. The regularity of the equal thickness fringes along each sample indicates the uniformity of the chemical composition in our samples.

V. PHOTOLUMINESCENCE MEASUREMENT

In Fig. 3 we present typical PL spectra of a MQW structure (sample *D*) measured at different temperatures from 4 to 304 K. The 4-K PL spectrum shows a dominant peak at 1.5596 eV ($E_{e1\text{-hh}}$) due to the radiative recombination of the $n=1$ electron–heavy-hole exciton confined in the quantum wells. The emission peak at 1.5159 eV (E_b) is due to the recombination of free excitons in the GaAs buffer layer. At this temperature, the $n=1$ electron–light-hole exciton recombination peak cannot be observed in the PL spectrum because of thermalization effects.[12] On the 78-K PL spectrum, besides the E_b (1.507 eV) and $E_{e1\text{-hh}}$ (1.549 eV) emission lines, a new emission line related to the $n=1$ electron–light-hole exciton recombination ($E_{e1\text{-lh}}$) appears at around 1.560 eV. The $n=2$ electron–heavy-hole exciton recombination line ($E_{e2\text{-hh}}$) arises on the high-energy side of the spectrum due to the thermal population of the $n=2$ heavy-hole excitonic state above 200 K.[11] The high-energy tails of the spectra at higher temperatures are consistent with the thermal population. All of the above observations are on the PL spectra of the other samples (*A*,*B*,*C*).

Considering that the values of L_w are identical for all of our MQW structures, we investigate the influence of the Al content x on the PL spectra. We find that the dependence of the transition energies $E_{e1\text{-hh}}-E_g$ and $E_{e1\text{-lh}}-E_g$ on x fits the relations (Fig. 4)

TABLE I. The parameters of the MQW structures obtained by x-ray diffraction, WTEM, and PL measurement.

	Sample *A*	Sample *B*	Sample *C*	Sample *D*	Technique
Al content x in barrier	0.085±0.01	0.19±0.01	0.465±0.01	1	X-ray diffraction
	0.103±0.01	0.206±0.01	0.447±0.01	1	WTEM
GaAs cap layer thickness	0.110 μm	0.114 μm	0.101 μm	0.111 μm	WTEM
Period L_w+L_b	331±3 Å	333±3 Å	293±4 Å	320±2 Å	X-ray diffraction
	330±6 Å	338±6 Å	297±6 Å	319±5 Å	WTEM
Well thickness L_w	112±3 Å	112±3 Å	97±4 Å	111±2 Å	X-ray diffraction
	116±6 Å	115±6 Å	104±6 Å	104±5 Å	WTEM
	113±3 Å	113±3 Å	107±3 Å	102±2 Å	PL
GaAs buffer layer thickness	0.398 μm	0.423 μm	0.398 μm	0.394 μm	WTEM

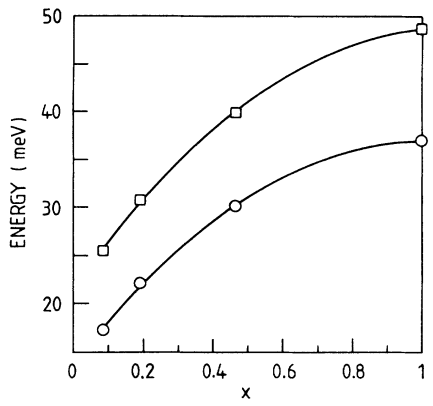

FIG. 4. Dependence of the transition energies $E_{e1\text{-hh}}-E_g$ (circles) and $E_{e1\text{-lh}}-E_g$ (squares) on the Al content x in the barriers.

$$E_{e1\text{-hh}}-E_g\ (\text{meV})=13.8+46x-22.9x^2\ , \tag{2}$$

$$E_{e1\text{-lh}}-E_g\ (\text{meV})=21.6+50.6x-23.6x^2\ . \tag{3}$$

For a transition in the MQW structure, for example $E_{e1\text{-hh}}$, we have[1]

$$E_{e1\text{-hh}}-E_g=E_{e1}+E_{\text{hh}}-E_{\text{ex}}^{\text{hh}}\ , \tag{4}$$

where E_g is the band-gap energy of GaAs, $E_{\text{ex}}^{\text{hh}}$ is the heavy-hole exciton binding energy in the well, E_{e1} is the energy of the $n=1$ electron subband edge above the conduction-band edge of the well, and E_{hh} and E_{lh} are the energies of the heavy-hole and light-hole subband edges below the valence-band edge of the well. The exciton binding energies can be obtained from the difference between the transition energies ($E_{e1\text{-hh}}-E_g$ or $E_{e1\text{-lh}}-E_g$) and the quantum confinement energies ($E_{e1}+E_{\text{hh}}$ or $E_{e1}+E_{\text{lh}}$).

We calculate the quantum confinement energies at the zone center within the effective-mass approximation using the formula[17]

$$\tan\left[\frac{m_{e,h}^{w}E_{e,h}L_w^2}{2\hbar^2}\right]^{1/2}=\left[\frac{(V_{e,h}-E_{e,h})m_{e,h}^{w}}{m_{e,h}^{b}E_{e,h}}\right]^{1/2}\ , \tag{5}$$

where $m_{e,h}^{w}, m_{e,h}^{b}$ are the effective mass of electrons (e) or holes (h) in the wells and barriers, respectively; $E_{e,h}$ is the confinement energy in the conduction or valence band (this means E_{e1} or E_{hh} or E_{lh}); $V_{e,h}$ is the height of the potential barrier for electrons and holes. We use the following parameters.

(i) Band-edge discontinuities: $\Delta E_c=Q\Delta E_g$ and $\Delta E_v=(1-Q)\Delta E_g$, where the conduction-band offset $Q=0.65$ (Refs. 18 and 19) and $\Delta E_g=E_g^b-E_g^w$.

(ii) The value ΔE_g (Γ band) of $Al_xGa_{1-x}As$ is determined by the equation[20]

$$\Delta E_g=1.36x+0.22x^2\ \text{eV}\ . \tag{6}$$

(iii) The effective mass of electrons in the conduction band m_e and of heavy holes and light holes in the valence band $m_{\text{hh}}, m_{\text{lh}}$ are[21,22] $m_e=0.0665m_0$, $m_{\text{hh}}=0.34m_0$, $m_{\text{lh}}=0.094m_0$ for GaAs; $m_e=0.15m_0$, $m_{\text{hh}}=0.4m_0$, $m_{\text{lh}}=0.18m_0$ for AlAs. The effective-mass values in the barrier with different Al content x are deduced from

$$m(x)=m(\text{GaAs})+[m(\text{AlAs})-m(\text{GaAs})]f\ , \tag{7}$$

where

$$f=[E_g(x)-E_g(\text{GaAs})]/[E_g(\text{AlAs})-E_g(\text{GaAs})]\ . \tag{8}$$

In Table II we give the confinement energy and exciton binding-energy values calculated using the best fit of the values L_w obtained by WTEM and x-ray diffraction and of the PL data. In Table III we present the exciton binding-energy values reported previously by different authors.[14,19,23-26] Our values of $E_{\text{ex}}^{\text{hh}}$ and $E_{\text{ex}}^{\text{lh}}$ are quite close to those determined from low-field magneto-optics by Rogers *et al.*[26] ($E_{\text{ex}}^{\text{hh}}=8\pm1$ meV and $E_{\text{ex}}^{\text{lh}}=9\pm1$ meV for $L_w=110$ Å, $x=0.35$) and to those calculated theoretically by Greene , Bajaj, and Phelps.[14] On the other hand, Andreani and Pasquarello[19] have recently performed an accurate theoretical calculation of $E_{\text{ex}}^{\text{hh}}$ and $E_{\text{ex}}^{\text{lh}}$ including the following effects: valence-band mixing, Coulomb coupling between excitons belonging to different subbands, nonparabolicity of the bulk conduction band, and the difference in dielectric constants between well and barrier materials. These effects increase the exciton binding energy: for $L_w=110$ Å and $x=0.4$, the values of $E_{\text{ex}}^{\text{hh}}$ and $E_{\text{ex}}^{\text{lh}}$ are 8.1 and 8.7 meV, respectively, without including the effects, whereas they are 9.5 and 12 meV including the effects. We use Eq. (4) to deduce the values of $E_{\text{ex}}^{\text{hh}}$ and $E_{\text{ex}}^{\text{lh}}$. Hence, the discrepancy between our values of $E_{\text{ex}}^{\text{hh}}$ and $E_{\text{ex}}^{\text{lh}}$ and those calculated by Andreani and Pasquarello[19] and Chang, Sanders, and Chu[24] could be due to the fact that we do not include the above effects in our calculation of the quantum confinement energies. The values of $E_{\text{ex}}^{\text{hh}}$ and $E_{\text{ex}}^{\text{lh}}$ extrapolated from high-field

TABLE II. The transition energies $E_{e1\text{-hh}}-E_g$ and $E_{e1\text{-lh}}-E_g$ obtained from PL data, the calculated confinement energies $E_{e1}+E_{\text{hh}}$ and $E_{e1}+E_{\text{lh}}$, the energy splitting between heavy-hole and light-hole subband edges $E_{\text{lh}}-E_{\text{hh}}$, and the heavy-hole $E_{\text{ex}}^{\text{hh}}$ and light-hole $E_{\text{ex}}^{\text{lh}}$ exciton binding energies.

	x	$E_{e1\text{-hh}}-E_g$ (meV)	$E_{e1\text{-lh}}-E_g$ (meV)	$E_{e1}+E_{\text{hh}}$ (meV)	$E_{e1}+E_{\text{lh}}$ (meV)	$E_{\text{lh}}-E_{\text{hh}}$ (meV)	$E_{\text{ex}}^{\text{hh}}$ (meV)	$E_{\text{ex}}^{\text{lh}}$ (meV)
Sample *A*	0.085	17.3	25.5	24	31.1	7.1	6.7±1	5.6±1
Sample *B*	0.19	22.1	30.7	30	39.8	9.8	7.9±1.2	9.1±1.5
Sample *C*	0.465	30.1	39.9	38.3	51.8	13.5	8.2±1.8	11.9±2.4
Sample *D*	1	37	48.7	45.5	61.9	16.4	8.5±1.5	13.2±2

TABLE III. The heavy-hole (E_{ex}^{hh}) and light-hole (E_{ex}^{lh}) exciton binding-energy values obtained by different authors for $L_w \approx 110$ Å using high-field magneto-optics (HFMO), low-field magneto-optics (LFMO), theoretical calculation including finite barrier height (*), and theoretical calculation including the following effects (**): valence-band mixing, Coulomb coupling between excitons belonging to different subbands, nonparabolicity of the bulk conduction band, and the difference in dielectric constants between well and barrier materials.

	E_{ex}^{hh} (meV)		E_{ex}^{lh} (meV)			
x	Theoretical	Experimental	Theoretical	Experimental	Technique	Reference
0.15		12		9.4	HFMO	a
	7.8		8		*	b
0.25	9		11		**	c
	9.1		11.2			d
0.29		13		10	HFMO	a
0.3	8.2	12			HFMO	e
	8		8.5		*	b
0.35	8.4	8±1	9.9	9±1	LFMO	f
0.4	9.5		12		**	c
	9.5		12.4			d
1	11		14		**	c

[a]Reference 23.
[b]Reference 14.
[c]Reference 19.
[d]Reference 24.
[e]Reference 25.
[f]Reference 26.

magneto-optics[23,25] are larger than ours and than those expected theoretically. The authors[23,25] explained this discrepancy by an experimentally determined reduced mass higher than that used in theoretical calculations. Our results show that the transmission energies $E_{e1\text{-hh}}-E_g$ and $E_{e1\text{-lh}}-E_g$ decrease as the Al content x decreases (Fig. 4) because the confinement energy and exciton binding energy decrease with decreasing x (Table II). With decreasing x, the spilling of the wave function in the surrounding $Al_xGa_{1-x}As$ barriers becomes more and more important. This makes the exciton binding energy decrease toward the value appropriate to the bulk barrier material.[14,19] We note that the exciton binding energy in bulk $Al_xGa_{1-x}As$ ($x=0.085$) is 5.4 meV according to the equation[27]

$$E_{ex}(x)=4+17x \text{ (meV)} . \quad (9)$$

Since the in-plane heavy-hole mass is less than that of the light hole, the binding energy of the light-hole exciton is expected to be greater than that of the heavy-hole exciton,[28] as is observed in Table II for $x \geq 0.19$. But for $x=0.085$ we find that E_{ex}^{lh} becomes smaller than E_{ex}^{hh}. This agrees with the theoretical results reported by Greene, Bajaj, and Phelps.[14] They have taken the finite barrier into account and show that for a given value of L_w, both values of E_{ex}^{hh} and E_{ex}^{lh} decrease as x is reduced. There is a certain critical value x_c at which the two values of E_{ex}^{hh} and E_{ex}^{lh} are equal and then E_{ex}^{lh} becomes smaller than E_{ex}^{hh}. The value of x_c depends on L_w; the larger L_w, the smaller the value of x_c. For $L_w=50$ Å, $x_c=0.3$. In Table II, we find $x_c<0.19$ for $L_w \approx 110$ Å. This is in contrast to the behavior of E_{ex}^{hh} and E_{ex}^{lh} calculated for infinite potential barriers where E_{ex}^{lh} is always larger than E_{ex}^{hh}.

The temperature dependence of the peak position of all transitions in the MQW layers and in the GaAs buffer layer is shown in Fig. 5. The $E_{e1\text{-hh}}$ and $E_{e1\text{-lh}}$ recombination peaks of MQW structures are significantly shifted to higher energy from that of the GaAs buffer layer E_b. With increasing temperature, all emission peaks shift to

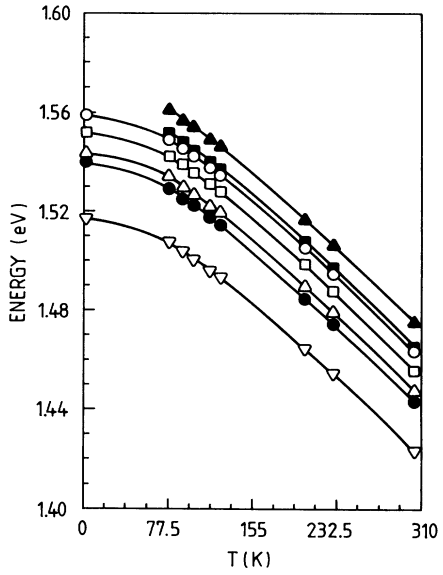

FIG. 5. Temperature dependence of the peak position of the recombination E_b in the GaAs buffer layer (blank inverse triangles), of the $n=1$ electron–heavy-hole exciton recombinations $E_{e1\text{-hh}}$ (full circles for sample A, blank triangles for sample B, blank squares for sample C, blank circles for sample D), and of the $n=1$ electron–light-hole exciton recombinations $E_{e1\text{-lh}}$ (full squares for sample C, full triangles for sample D) in the MQW structures.

the low-energy side in the same way. Theoretical results[18] show that the subband energies E_{e1}, E_{hh}, and E_{lh} as well as the binding energy of heavy-hole and light-hole excitons are almost independent of temperature because the temperature affects primarily the energy gap. We do not observe the change from excitonic to band-to-band transitions for the $E_{e1\text{-}hh}$ and $E_{e1\text{-}lh}$ curves. However, above 200 K the differences $E_{e1\text{-}hh}-E_b$ and $E_{e1\text{-}lh}-E_b$ slightly decrease. This decrease could indicate a change of the recombination mechanism from excitonic to band-to-band in the GaAs buffer layer. In the GaAs buffer layer where the exciton binding energy is about 4 meV, the population of electrons and holes in the conduction and valence bands increases considerably due to thermal dissociation of excitons. As a consequence, the recombination mechanism changes. By contrast, the values of the exciton binding energy in the MQW structures are theoretically and experimentally found to be higher. Hence, excitonic states remain stable up to room temperature.

The excitonic character of the observed recombinations is confirmed by the excitation dependence of PL-integrated intensity, Fig. 6. The PL-integrated intensity I_{PL} can be written as[10]

$$I_{PL}=CI_{exc}^{\alpha}\ , \tag{10}$$

where I_{exc} is the excitation intensity and C is a constant. The exponent α depends on the recombination mechanism. An analysis of Fouquet and Siegman[29] indicated that for an excitonic recombination $\alpha=1$, whether radiative or nonradiative recombination dominates, whereas for free-carrier recombination $\alpha=2$ assuming that nonradiative recombination dominates in undoped materials. The nonradiative recombination could be due to many factors, for example the recombination through interface states between the well and barrier regions.[29] An intermediate case involving free excitons and free carriers yields a value of α between 1 and 2. In our case, the nominally undoped MQW structures are sandwiched between 0.1 μm (above) and 0.4 μm (below) undoped GaAs layers. We found that the peak position does not change with increasing excitation intensity. The values $\alpha=1.16-1.29$ at 77 K and $\alpha=1.41-1.53$ at 304 K indicate that at low temperature, the excitonic recombination is dominant. Free excitons dominate the recombination process up to room temperature but free carriers are also present at room temperature. Our results agree with those of Fujiwara, Tsukada, and Nakayama.[30] They observed the recombination involving free excitons at room temperature in GaAs single quantum wells with $\alpha=1.65$. Moreover, Colocci, Gurioli, and Vinattieri[31] recently reported that although an accurate fit of the PL line shape indicates the presence of free-carrier recombination, the PL peak is related to free-exciton recombination up to 300 K.

The temperature dependence of the full width at half maximum (FWHM) is shown in Fig. 7 for the E_b line and the $E_{e1\text{-}hh}$ line of all samples. The FWHM of the E_b line increases quickly with increasing temperature. It indicates the thermal dissociation of excitons in the GaAs buffer layer. However, the FWHM of the $E_{e1\text{-}hh}$ lines shows the same temperature dependence for the MQW structures: it varies slowly up to about 150 K and then increases rapidly. The above results agree well with those reported by other authors.[9-12,32,33] The linewidth Γ of the exciton lines is given by Chemla *et al.*[33] as

$$\Gamma=\Gamma_0+\Gamma_1\ , \tag{11}$$

where Γ_0 represents the local fluctuation in the L_w, Γ_1 is proportional to the density of thermal LO phonons with proportionality constant Γ_{ph},

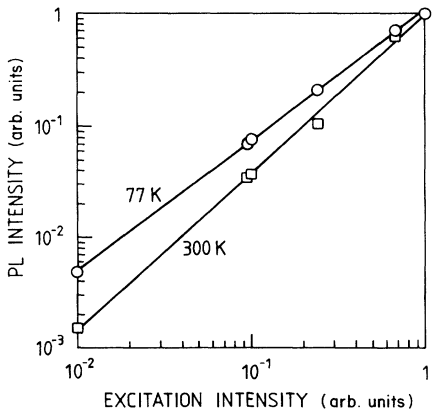

FIG. 6. Excitation dependence of integrated photoluminescence intensity at 77 K (circles) and 300 K (squares).

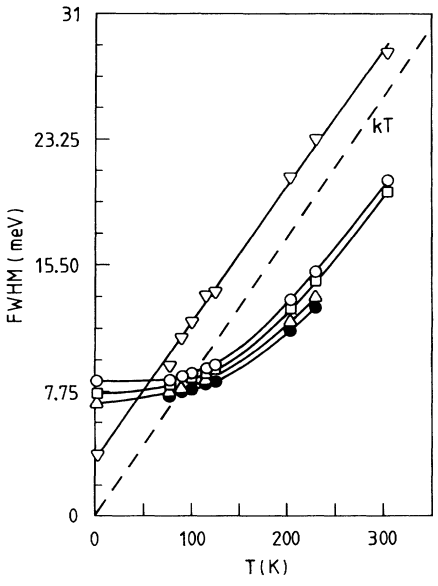

FIG. 7. Temperature dependence of the full width at half maximum (FWHM) of the E_b and $E_{e1\text{-}hh}$ emission lines. The symbols in this figure correspond to those of Fig. 5.

$$\Gamma_1 = \frac{\Gamma_{ph}}{\exp(\hbar\omega_{LO}/kT)-1} , \quad (12)$$

$\hbar\omega_{LO}$ is the GaAs-type LO phonon energy. Equations (11) and (12) show that the main contributions to the linewidth of excitons is attributed to unavoidable inhomogeneous fluctuations in the well thickness and to lattice interactions via LO phonons. On the other hand, a theoretical model of Lee, Kofeles, and Vassell[32] predicts that the interactions between heavy-hole and/or light-hole excitons and acoustic phonons (LA) or polar optical phonons (LO) contribute to the linewidth. At low temperatures LA phonon scattering is the dominant mechanism and the linewidth is proportional to the LA phonon population which depends linearly on T. In the low-temperature range, LO phonon population is negligible, whereas at $T > 200$ K the linewidth increases rapidly because LO phonon scattering becomes the dominant mechanism. The LO phonon population increases with T corresponding to Eq. (12). The temperature dependence of FWHM of our MQW structures can be explained by both of the above models.[32,33] At low temperatures the values of FWHM increase from 7.0 ($x = 0.085$) to 8.4 meV ($x = 1$). The large values of FWHM of the MQW structures indicate that in our case the contribution of the inhomogeneous fluctuations in the well thickness to the linewidth could be important. The inhomogeneous fluctuations in the thickness of the wells are due to the roughness of the interfaces between GaAs and $Al_xGa_{1-x}As$ layers. For good quality samples, the magnitude of the thickness fluctuations is one atomic monolayer.[1,34] The real QW layer seems to be an assembly of lateral islands within each of which L_w is uniform. When the lateral size of the island is larger than the exciton size, the PL spectrum has a multiple peak structure with different peak energies from different islands. When the island size is smaller than the exciton size, an exciton experiences different values of L_w, giving a broadening of the PL line.[1,35] By annealing our MQW structures at 600 °C for 4 h in an As overpressure, we observe a FWHM reduction of 0.5–1 meV on the 77-K PL spectra of the MQW structures. This fact confirms that the linewidth broadening is due to the interface roughness. In Fig. 7, the rise in the values of FWHM with increasing x at a given temperature indicates that the GaAs/$Al_xGa_{1-x}As$ interfaces are rougher for the materials with the higher value of x. A theoretical study[36] of the quality of GaAs/$Al_xGa_{1-x}As$ interfaces grown by MBE pointed out that the interface roughness is controlled by the surface migration of Ga and Al atoms. Due to the high migration rates of Ga atoms the growth front continues to remain flat during GaAs growth. The $Al_xGa_{1-x}As$-on-GaAs interface is expected to be pseudosmooth and sharp to a monolayer. The quality of the GaAs-on-$Al_xGa_{1-x}As$ interface is controlled by the $Al_xGa_{1-x}As$ surface quality that depends on the Al migration rate and on the Al concentration. The strong Al-As bond leads to a low value of Al migration rate. Hence, the GaAs-on-$Al_xGa_{1-x}As$ interface would be rough to about four monolayers.[36] In a previous work,[8] we found that the interface roughness has an important influence on the optical properties of the AlAs/GaAs superlattice. The experimental results of Tanaka, Sakaki, and Yoshino[37] show that the PL linewidth broadening is mainly due to the roughness of the GaAs-on-$Al_xGa_{1-x}As$ interface. The linewidth broadening increases with increasing x.[1,37]

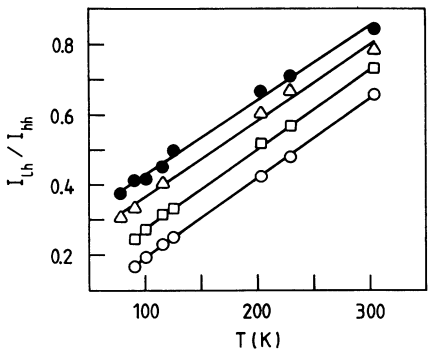

FIG. 8. Temperature dependence of the intensity ratio between the $E_{e1\text{-}lh}$ and $E_{e1\text{-}hh}$ emission lines I_{lh}/I_{hh}. The symbols in this figure correspond to those of Fig. 5.

Because the binding energy of the $E_{e1\text{-}hh}$ exciton is lower than that of the $E_{e1\text{-}lh}$ exciton, the thermal dissociation of $E_{e1\text{-}hh}$ excitons is stronger than that of $E_{e1\text{-}lh}$ excitons. Hence the increase in the intensity ratio of the $E_{e1\text{-}lh}$ and $E_{e1\text{-}hh}$ emission lines I_{lh}/I_{hh} with increasing temperature is observed (Fig. 8). The free carriers produced by the thermal dissociation of excitons coexist with excitons following the two-dimensional (2D) law of mass action.[31] They contribute to the band-to-band recombination and induce the broadening of the emission line. In Fig. 8, we note that the temperature dependence of the I_{lh}/I_{hh} ratio of all MQW structures has the same behavior. In Table II we observe an increase in the energy splitting between the heavy-hole and light-hole subband edges with increasing x. This explains the fact that at a given temperature, the I_{lh}/I_{hh} ratio is higher for the sample with lower Al content x in the barrier. The I_{lh}/I_{hh} ratio also increases as the excitation intensity increases due to the increase of light-hole exciton population.

VI. CONCLUSION

We have characterized the GaAs/$Al_xGa_{1-x}As$ MQW structures ($x = 0.1-1$) with $L_w \approx 110$ Å by a combination of different techniques. X-ray diffraction and WTEM are shown to be very useful and complementary techniques for observing and determining the key parameters of the MQW structures such as x, L_w, L_b, and uniformity. The PL data obtained for a wide range of temperature show the coexistence of excitons and free carriers at high temperatures, but the excitonic recombination is dominant up to room temperature. This gives evidence for the high quality of the MQW structures. The PL properties as a function of x are also investigated. Our data confirm the

theoretical results calculated using finite barrier heights and show that the increase of transition energies with increasing x is due to the increase of confinement energies and exciton binding energies. The structure parameters obtained by the above techniques are in good agreement.

ACKNOWLEDGMENTS

The authors wish to thank the Swiss National Science Foundation and Thomson-CSF for the financial support. We also thank Y. Magnenat for her technical support.

[1]H. Okamoto, Jpn. J. Appl. Phys. **26**, 315 (1987).

[2]T. Ishibashi, Y. Suzuki, and H. Okamoto, Jpn. J. Appl. Phys. **20**, L623 (1981).

[3]G. T. Baumbach, G. Oelgart, P. von Allmen, F. Morier-Genoud, D. Martin, J. D. Ganière, and F. K. Reinhart (unpublished). See also G. T. Baumbach, G. Oelgart, H. G. Brühl, U. Pietsch, E. Tuncel, F. Morier-Genoud, D. Martin, F. K. Reinhart, and B. Lengeler, Semicond. Sci. Technol. **7**, 304 (1992).

[4]H. Kakibayashi and F. Nagata, Jpn. J. Appl. Phys. **24**, L905 (1985).

[5]P. Ossart, M. J. S. P. Brasil, L. P. Cardoso, J. D. Ganière, L. Horiuchi, J. Decobert, and M. Sacilotti, Jpn. J. Appl. Phys. **30**, L783 (1991).

[6]P. A. Buffat, J. D. Ganière, and P. Stadelmann, *Evaluation of Advanced Semiconductor Materials by Electron Microscopy* (Plenum, New York, 1990), p. 319.

[7]A. Ougazzaden, J. D. Ganière, Y. Gao, E. V. K. Rao, B. Sermage, C. Kazmierski, and A. Mircea, J. Cryst. Growth **107**, 761 (1991).

[8]J. Faist, J. D. Ganière, P. Buffat, S. Sampson, and F. K. Reinhart, J. Appl. Phys. **66**, 1023 (1989).

[9]P. Dawson, G. Duggan, H. I. Ralph, and K. Woodbridge, Phys. Rev. B **28**, 7381 (1983).

[10]Xu Zhongying, Xu Jizong, Ge Weikun, Zheng Baozhen, Xu Junying, and Li Yuzhang, Solid State Commun. **61**, 707 (1987).

[11]R. Cingolani, Y. Chen, and K. Ploog, Europhys. Lett. **6**, 169 (1988).

[12]Y. Chen, R. Cingolani, L. C. Andreani, F. Bassani, and J. Massies, Il Nuovo Cimento **10D**, 847 (1988).

[13]G. Bastard, *Wave Mechanics Applied to Semiconductor Heterostructures* (Les Édition de Physique, New York, 1988), p. 93.

[14]R. L. Greene, K. K. Bajaj, and D. E. Phelps, Phys. Rev. B **29**, 1807 (1984).

[15]M. S. Goorsky, T. F. Kuech, M. A. Tischler, and R. M. Potemski, Appl. Phys. Lett. **59**, 2269 (1991).

[16]B. K. Tanner, A. G. Turnbull, C. R. Stanley, A. H. Kean, and M. McElhinney, Appl. Phys. Lett. **59**, 2272 (1991).

[17]M. A. Herman, D. Bimberg, and J. Christen, J. Appl. Phys. **70**, R1 (1991).

[18]D. S. Chuu and Y. C. Lou, Phys. Rev. B **43**, 14 504 (1991).

[19]L. C. Andreani and A. Pasquarello, Phys. Rev. B **42**, 8928 (1990).

[20]C. Bosio, J. L. Staehli, M. Guzzi, G. Burri, and R. A. Logan, Phys. Rev. B **38**, 3263 (1988).

[21]S. Adachi, J. Appl. Phys. **58**, R1 (1985).

[22]D. F. Nelson, R. C. Miller, C. W. Tu, and S. K. Sputz, Phys. Rev. B **36**, 8063 (1987).

[23]J. C. Maan, G. Belle, A. Fasolino, M. Altarelli, and K. Ploog, Phys. Rev. B **30**, 2253 (1984).

[24]Y. C. Chang, G. D. Sanders, and H. Y. Chu, *Excitons in Confined Systems* (Springer-Verlag, New York, 1988), p. 189.

[25]M. Altarelli, *Excitons in Confined Systems* (Springer-Verlag, New York, 1988), p. 181.

[26]D. C. Rogers, J. Singleton, R. J. Nicolas, C. T. Foxon, and K. Woodbridge, Phys. Rev. B **34**, 4002 (1986).

[27]L. Pavesi, *Properties of Gallium Arsenide* (INSPEC, Institution of Electrical Engineers, New York, 1990), p. 529.

[28]R. C. Miller and D. A. Kleinman, J. Lumin. **30**, 520 (1985).

[29]J. E. Fouquet and A. E. Siegman, Appl. Phys. Lett. **46**, 280 (1984).

[30]K. Fujiwara, N. Tsukada, and T. Nakayama, Appl. Phys. Lett. **53**, 675 (1988).

[31]M. Colocci, M. Gurioli, and A. Vinattieri, J. Appl. Phys. **68**, 2809 (1990).

[32]J. Lee, E. S. Koteles, and M. O. Vassell, Phys. Rev. B **33**, 5512 (1986).

[33]D. S. Chemla, D. A. B. Miller, P. W. Smith, A. C. Gossard, and W. Wiegmann, IEEE J. Quantum Electron. **QE-20**, 265 (1984).

[34]B. Deveaud, J. Y. Emery, A. Chomette, B. Lambert, and M. Baudet, Appl. Phys. Lett. **45**, 1078 (1984).

[35]D. C. Reynolds, K. K. Bajaj, C. W. Litton, J. Singh, P. W. Yu, P. Pearah, J. Klem, and H. Morkoc, Phys. Rev. B **33**, 5931 (1986).

[36]J. Singh and K. K. Bajaj, J. Vac. Sci. Technol. B **3**, 520 (1985).

[37]M. Tanaka, H. Sakaki, and J. Yoshino, Jpn. J. Appl. Phys. **25**, L155 (1986).

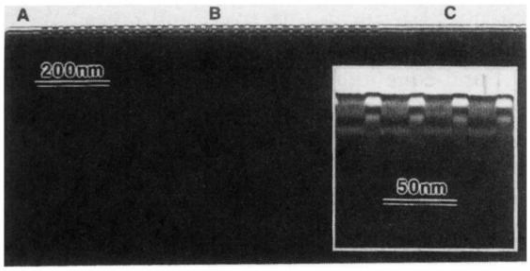

FIG. 2. WTEM photograph of sample *C*. The growth direction is from the right to the left. In this figure, the letter A indicates the GaAs cap layer, B the MQW region, and C the GaAs buffer layer.